Title	Influence of Substrate on Plasmon-Induced Absorption Enhancements
Author(s)	Tappura, Kirsi; Luomahaara, Juho; Haatainen, Tomi; Hassel, Juha; Vehmas, Tapani
Citation	Plasmonics . Springer. Vol. 11 (2016) No: 2, Pages: 627-635
	This is a post-peer-review, pre-copyedit version of an article published in Plasmonics. The final authenticated version is available online at: http://dx.doi.org/10.1007/s11468-015-0090-4
Date	17.1.2018

Influence of substrate on plasmon-induced absorption enhancements

K. Tappura,*[a] J. Luomahaara,[b] T. Haatainen,[b] J. Hassel[b] and T. Vehmas[b]

*to whom correspondence should be address
[a]VTT Technical Research Centre of Finland. P.O. Box 1300, FI-33101 Tampere, Finland
[b]VTT Technical Research Centre of Finland, P.O. Box 1000, FI-02044 VTT, Finland

Contact details for the corresponding author:
kirsi.tappura@vtt.fi, Tel: +358407041773, Fax: +358207223499

KEYWORDS: plasmonics; thin-film silicon; silicon-on-insulator; absorption enhancement; Fabry-Perot interference; multiple resonances

Abstract A set of periodic plasmonic nanostructures is designed and fabricated as a means to investigate light absorption in single-crystal silicon thin-film structures with silicon-on-insulator (SOI) wafers as a model system. It is shown both computationally and experimentally that plasmon-induced absorption enhancement is remarkably higher for such devices than for thick or semi-infinite structures or for the thin-film amorphous silicon solar cells reported in the literature. Experimental photocurrent enhancements of the order 12 and 20 are demonstrated for non-optimized 2200 nm thick photoconductive and 300 nm thick photovoltaic test structures, respectively. Theoretical absorption enhancements as high as 80, are predicted to be achievable for the similar structures. The features of the spectral enhancements observed are attributed to several interacting resonance phenomena: not just to the favourable scattering of light by the periodic plasmonic nanoparticle arrays into the SOI device layer and coupling to the waveguide modes interacting with the plasmonic array, but also to the Farby-Perot type interferences in the layered structure. We show that the latter effect gives a significant contribution to the spectral features of the enhancements, although frequently ignored in the discussions of previous reports.

Introduction

While designing photodetector structures or solar cells, the optimal device performance often tends to set contradictory demands for the thickness of the component [1-3]. To achieve efficient charge collection before recombination, the device structures should be as thin as possible. Thin-film devices are also desirable for fast detection and for the reduced material consumption and, thus, potentially reduced costs. On the other hand, active layers should be thick to enable efficient absorption of light. The coupling of light into a device is traditionally improved by multilayer antireflection coatings or by texturing the front surface of the device to scatter and trap light into the absorbing layer [4-5]. The conventional micrometer-scale texturing, however, cannot be used for thin-film devices due to the fact that the produced surface roughness may exceed the device thickness or at least increase significantly the minority carrier recombination. Alternative methods to enhance absorption without increasing the device thickness are, thus, required.

Over the last several years, a great deal of research effort has been put into the development of plasmonic nanostructures for enhancing light absorption in solar cells [6]. Metallic nanoparticles deposited on the front or rear surface of a semiconductor substrate have been shown to improve the absorption of light in various photovoltaic devices [7-10]. The main idea in such approaches has been to engineer the scattering cross-section of the plasmonic nanoparticles such that most of the light is scattered into the substrate with favourable angles and the part scattered in air or absorbed by the particle is minimized. The main features of these phenomena can be understood by approximating the plasmonic nanoparticle by a dipole. When placed close to a dielectric interface a dipole radiates most of its energy to the material with a higher refractive index due to its higher number of available states [11]. It is also known that the fraction, as well as the spatial distribution, of the emission into the high-index substrate depends on the distance of the dipole from the interface [11, 12]. Thus, the desired scattering (radiating) properties can be obtained by varying the size, shape, inter-particle distance and material of the plasmonic nanoparticle as well as the dielectric environment of the plasmonic structures. Additional design parameters can be obtained by the inclusion of periodic structures [10]. With successful designs the reflection losses can be reduced and the optical path of photons in the absorbing layer increased so that the probability for absorption enhances [6].

Efficient light trapping with the aid of plasmonics has been demonstrated for various thin-film structures both theoretically and experimentally [10, 13]. Due to the fact that amorphous silicon (Si) is widely used in thin-film solar cells, many of the plasmonics related thin-film studies have concentrated on such systems [9, 10]. Different levels of theory have been applied to various plasmonic device structures and materials [9, 14, 15], including the popular investigations where the surface of a semi-infinite substrate is mimicking the plamonic device [7, 8, 16]. Plasmonic nanoparticles have also been applied to (single crystal) silicon-on-insulator (SOI) photodetector and solar cell structures [1, 10, 17-19]. These studies report experimental photocurrent or

photoluminescence enhancements ranging from 2 to 18 and the maximum theoretical absorption enhancements, at the device-specific wavelengths, varying from 10 to 45. The high enhancements have been attributed to the plasmonic coupling of light into the waveguide modes of the SOI device [17].

Thin plasmonic SOI structures are especially interesting for photodetectors due to their potential for providing fast response speeds without the need to compromise the sensitivity, as well as for the possibility of monolithic integration with high-performance Si electronics. Although Si based thin-film solar cells are mostly fabricated from microcrystalline or amorphous Si, SOI structures provide a good model system also for them due to the fact that the phenomena related to light trapping can be seen very strongly in such single-crystal thin-film systems [10]. In spite of all the efforts reviewed above, the existence of Fabry-Pérot interferences in SOI waveguide structures is not discussed in combination with the plasmon-induced absorption enhancements or their influence to the spectral features considered. Instead, a study concentrating on thin-film solar cells with a corrugated metal film on the back interface shows the contribution of the photonic Fabry-Pérot effect [20]. Experimental demonstrations of absorption enhancements in single-crystal Si thin-films induced by periodic plasmonic nanostructures are also rare, different from the reports on random plasmonic nanostructures: While a ten-fold enhancement in photoluminescence spectra has been demonstrated [10], there appear to be no reports on photocurrent enhancements measured in thin-film crystalline Si induced by periodic plasmonic nanostructures.

In this paper, we investigate the influence of periodic plasmonic nanostructures on the enhancement of light absorption in 2200 and 300 nm thick single-crystal Si thin-films with SOI structures as model systems and compare the behaviour to that in bulk Si and to the thin-film amorphous Si results in the literature. The absorption enhancements are extracted from full three-dimensional electromagnetic (EM) simulations performed for realistic – computationally demanding, multilayer – SOI structures with plasmonic nanoparticles on top. The results are compared with the experimental spectral photocurrent enhancements measured for photoconductive and photovoltaic SOI based test devices. In addition to the plasmonics effects, strong photonic Fabry-Pérot resonances are observed both in the experimental SOI structures and in the results of the corresponding computational simulations. The Fabry-Pérot interferences are shown to highly complicate the interpretation of the results due to their sensitivity to the thickness variations in the multilayer structures. Nevertheless, it is demonstrated that the EM simulations are able to reproduce the main features of the spectral absorption enhancements shown in the experimental data. Further, it is shown that the overall enhancement of light absorption, induced by periodic plasmonic nanostructures, is much stronger in the SOI structures than in bulk single-crystal Si with the similar plasmonic surfaces, and the causes for the differences are discussed.

Methods

Computational

Numerical simulations were performed for a set of selected systems to predict the plasmonic-induced coupling of light into Si substrates. Periodic arrays of silver (Ag) nanoparticles (nanodots) were studied both on SOI and semi-infinite crystalline Si substrates (Figs. 1a-b). Two different SOI structures were studied computationally: one with the device layer thickness (h_{SOI}) of 2200 nm and the other one with 300 nm. The thicknesses of the buried oxide layer (h_{BOX}) were 500 nm and 3000 nm, respectively. The handle wafer was considered semi-infinite or thick enough to absorb all the light that may enter in it. A silicon dioxide (SiO_2) spacer layer of 30 nm or 50 nm in thickness (t_{OX}) was applied between the particles and the Si surface, similar to the passivation layers used in the experimental structures. The full three-dimensional (3D) Maxwell equations were solved by discretizing the fields on a grid by the finite element method (FEM) with perfectly matched layer (PML) boundary conditions [21]. Plane waves normally incident from air to the substrate surface (in the *z*-direction) were applied for excitation. Periodic boundary conditions (PBC) were used to form a square lattice with equal periods in the *x*- and *y*-directions. The simulated Ag nanoparticles were either plain cylinders or cylinders with a rounded (elliptical) top, with a chrome (Cr) adhesion layer of 2 nm in thickness between Ag and SiO_2, similar to the experimental structures. The particle diameter (*d*) was varied from 150 to 200 nm while the height was fixed to 150 nm. The dispersive optical constants were obtained from references 22, 23, 24 and 25 for SiO_2, Cr, Ag and Si, respectively.

Starting from the fact that the overall absorption, or dissipation of energy, in a material can be described by the divergence of the Poynting vector, $\boldsymbol{S}$:

$$\nabla \cdot \langle \boldsymbol{S}(\boldsymbol{r},\boldsymbol{\omega}) \rangle = -\frac{1}{2} Im[\omega \boldsymbol{P}(\boldsymbol{r},\boldsymbol{\omega}) \boldsymbol{E}^*(\boldsymbol{r},\boldsymbol{\omega})] \qquad (1)$$

where ω is the angular frequency of light, $\boldsymbol{r}$ the position, $\boldsymbol{P(r,\omega)}$ the polarization and $\boldsymbol{E}$ the electric filed, the time-average spectral power density absorbed, Q_{abs}, in volume V can be shown to be proportional to the electric field intensity and the imaginary part of the permittivity, $\varepsilon(\omega)$, if the materials are assumed to be linear and non-magnetic:

$$Q_{abs}(\omega) = \frac{\omega}{2} \int_V Im[\varepsilon(\omega)] |\boldsymbol{E}|^2 dV \qquad (2)$$

Equation (2) is used to calculate the power absorbed in silicon.

In addition to the FEM simulations, the transfer matrix method [26] was also used for the SOI structures without nanodots for fast evaluation of the fraction of light absorbed in the SOI device layer and for that of reflected from the surface.

Sample preparation

As a substrate in the experiments, we used two types of 150 mm diameter SOI wafers, one type with h_{SOI} = 2200 nm and h_{BOX} = 500 nm and the other one with h_{SOI} = 300 nm and h_{BOX} = 3000 nm. The SOI device layers of the substrates were p-type (Boron) with a nominal resistivity of 4-8 Ohm-cm and > 500 Ohm-cm, respectively.

The 2200 nm SOI wafers were prepared for photoconductivity measurements as follows. First, PECVD oxide was grown on to the substrate with a thickness of 50 nm. In the first lithography layer contact pads and alignment marks were defined onto substrate by direct laser writing into photoresist using Microtech Laserwriter. For the contacts the oxide layer was opened in BHF wet etch through the openings defined in the resist. A 150 nm thick aluminium layer forming the contact pads and the alignment marks were prepared onto the substrate using an MRC sputtering system and lift off. The size of the contact pads was 500 µm by 800 µm with a 150 µm wide gap reserved in between for the nanodot patterns. With the aim to form ohmic contacts in the Al-Si interface, the substrates were subjected to a thermal treatment in argon atmosphere for several hours with the temperature reaching 500 °C at maximum [27].

For patterning nanodots between the contact pads, the substrate was coated with a 220-240 nm layer of positive e-beam resist (PMMA). The nanodots were defined by a high resolution e-beam lithography tool (Vistec EBPG5000pESc). The diameter and pitch of the dots were varied in different samples, so that the diameter of the circular nanopatterns (d) was between 150-200 nm and the array formed a square matrix with a pitch (p) varied between 350-470 nm. After developing the exposed resist, 2 nm of Cr and 150 nm of Ag were evaporated onto samples prior to lift off. A scanning electron microscope (SEM) image of a nanodot matrix (with the nominal values of d = 180 nm and p = 420 nm) is shown in Fig. 1c.

In the final step, the nano-patterned areas with contact pads were isolated from the rest of the silicon device layer by forming a 10 µm wide trench around the device. The trench was patterned using a resist mask patterned by direct laser writing and plasma etching to open through the PECVD oxide mask and device Si layer down to the buried oxide. Finally, the substrates were diced into 5 mm by 5 mm chips.

In addition to the 2200 nm thick SOI samples, a SOI wafer with h_{SOI} = 300 nm, and a 30 nm PECVD LTO oxide on top (t_{OX}), was prepared for photovoltaic measurements. For these samples interdigitated contact areas were opened in the top oxide on the n- and p-junctions formed by arsenic and boron implantation, respectively, before depositing the Si-doped Al contact metals. The width of the metal fingers was 14 µm, the distance between their edges 33 µm and the total device area 10 mm^2. The plasmonic nanodot arrays (with d = 200 nm and p = 470 nm assembled in a square matrix format) were prepared on the 30 nm top oxide between the fingers as described above. Although the electrode design was by no means optimal for the efficiency due to the unnecessarily large area

(30%) covered by the electrodes, the device served as a suitable test platform for the studies of the influence of plasmonics nanostructures on light absorption in such thin SOI photovoltaic devices.

Measurements

In total sixty 2200 nm thick SOI samples (20 reference samples and 40 samples with nanodots) were fabricated and characterized as a means to investigate plasmonic light absorption in silicon. The IV characteristics of each sample were first measured in dark after which their responsivity to light at wavelengths 500-1100 nm was determined. A halogen lamp was used to produce wideband illumination that was passed through a chopper (with a frequency of 210 Hz) and a monochromator (Bentham TMc300) to select the wavelength of interest to be applied onto the sample. A small voltage-bias was used in the measurements. The signal from the sample was amplified with a low-noise transimpedance amplifier (Femto DDPCA 300) and lock-in detected with the reference signal arriving from the chopper to obtain the generated photocurrent. A typical IV curve shown in Fig. 1d illustrates two regimes of operation. The ohmic behaviour suggests that the resistivity of the SOI device layer limits the current at small bias voltages and the device can be treated as a photoconductive detector. This was ensured by measuring the geometry dependency of the zero-bias resistance $R_0 = \frac{\partial U}{\partial I}|_{\mathrm{U}=0}$ at different contact pad distances. At higher voltages the Schottky barrier between silicon and aluminium bonding pads comes into play [28]. Computation of the mean zero-bias resistance $\langle R_0 \rangle = 13.6 \pm 0.9$ kΩ implies that the actual variations in h_{SOI} remain below 7 percent. However, even small changes in h_{SOI} will influence spectral absorption considerably and, therefore only samples with identical R_0 were compared. The photovoltaic devices were measured with the same methods and setup as described above but without bias voltage.

Results and discussion

To study the influence of plasmonic nanostructures on light absorption in SOI device layers, the different arrays of Ag nanodots prepared on SOI wafers were compared to the simulations of the corresponding structures on SOI and semi-infinite Si substrates. The absorption (simulations) and photocurrent (experiment) enhancement in a SOI device layer of 2200 nm in nominal thickness, is shown in Fig. 2a-d. The enhancement is induced by three different nanodot arrays assembled in periodic formats on a 50 nm top oxide layer. In Figs. 2a-c d = 150 nm and in Fig. 2d d = 180 nm. The height of all the nanodots is 150 nm. The pitch in the square matrix is 350 nm, 450 nm and 420 for Figs. 2a, 2b-c and 2d, respectively. The thickness of the surface oxide or the details of the Ag nanostructures were not optimised. However, the selected dimensions give fairly high absorption enhancements as compared to a set of additional simulations (not shown) and, thus, are expected to give a good insight into the potential of the absorption enhancements achievable. All the simulated

nanodots on the SOI structures were cylinders with a rounded top in shape (dot 2), while the simulations with semi-infinite substrates were performed for both sharp (dot 1) and rounded-top (dot 2) cylinders. Comparison of the simulated and the experimental spectra at wavelengths below 600 nm suggests that the fabricated Ag nanodots may not be perfectly sharp cylinders with sharp edges as could be expected for an ideal nanofabrication process. Instead, some variation in the shape of the nanodots is assumed with somewhat rounded or faceted top. This conclusion is also supported by AFM measurements (not shown). A plasmon-induced reduction in the absorption (absorption enhancement < 1) can also be seen at short wavelengths. This can be attributed to a destructive interference between scattered and incident light occurring at wavelengths below the plasmon resonance (Fano effect) [10, 29]. The different behaviour of the sharp and rounded top cylinders has its origin in the different (wavelength dependent) near-field distributions, which modifies the scattering properties of the particle arrays and, thus, the coupling of light into the substrate in combination with the Fano effect.

The measured absorption enhancement − plotted as a function of wavelength in Fig. 2a-d − is defined as the ratio of the photocurrent generated in the SOI device layer under the nanodotted area to that of a device without the dots. The corresponding simulation results of the SOI structures are also depicted in Figs. 2a-d. In the simulations the absorption enhancement is defined as the ratio of the power absorbed in Si (or in the SOI device layer) for the device with the nanodots to that without the dots. Thus, no recombination losses are considered in the simulations but all the generated electron-hole pairs are assumed to contribute to the photocurrent of a device. This assumption is justified as long as the recombination rates and processes in silicon are not somehow influenced by the addition of the nanodots on top, i.e. the effect of the recombination losses are cancelled out while calculating the absorption enhancements. In Figs. 2a-d, the calculated absorption enhancements are also shown for the corresponding nanodots on semi-infinite Si substrates.

Strong oscillations are clearly visible in both the experimental and computational enhancement spectra of the SOI structures. It is also evident that the plasmonic induced absorption enhancement is remarkably higher in the SOI devices than in the semi-infinite ones with the similar surface structures and illumination. With the selected Ag nanostructures and the thickness of the surface oxide layer, the maximum absorption enhancements always remain below 1.4 for all the simulated structures on the semi-infinite substrates, while the values for the SOI substrates vary from 3.8 to 11.6 for the experimental samples and from 5 to 80 for the simulated spectra. The difference between the experimental and the simulated results can be explained by the combination of several factors: the spatial inhomogeneity of the experimental samples (affecting, among other things, to the depth and width of the Fabry-Pérot resonances and waveguide coupling), the finite effective bandwidth of the monochromator (5 nm) used in the photocurrent measurements, as well as the deviation of the actual structural and material parameters from the ones used in the simulations. It is also possible that the inevitable recombination losses − neglected in the simulations − are higher in the plasmonic

samples than in the references, due to the nanofabrication process or the different spatial distribution of the (high) electric field among the bulk-like and the near surface/interface regions of the SOI device layer.

The exact peak positions of the oscillations also vary somewhat in the computational and experimental curves. This is an expected result, as well, due to the sensitivity of the Fabry-Pérot resonances – originating from the reflections of light at the interfaces of the multilayer structure – to the layer thicknesses. To highlight this, Fig. 2e compares the fraction of light absorbed in the device layer of a similar SOI structure as the ones in Figs. 2a-d but without nanodots, with the fraction of light absorbed in a structure where the thicknesses of the SOI device layer is changed by 50 nm. It can be seen that the envelope of the oscillations remains roughly the same but the spectral positions of the peaks are significantly shifted relative to each other. Another demonstration of the sensitivity of the peak positions to the layer thicknesses is the differences of the simulated spectra in Figs. 2b and 2c. According to the specifications of the manufacturer of the SOI wafers, the thickness variations can be fairly high (up to ±500 nm) and, thus, the device layer thicknesses of the experimental samples are likely to differ from the nominal thicknesses used in the simulations. When the SOI device layer is made thicker, a broad band increase in the absorbance is also detected as expected due to the increase in the absorbing volume (only faintly visible in Fig. 2e as the change in the thickness is very small).

The amplitude of the oscillations in the absorption enhancement is higher at longer wavelengths close to the band gap of Si. This can be understood by the lower absorption coefficient of silicon at longer wavelengths: While the high energy photons are effectively absorbed already in the very thin surface regions, the longer wave radiation passes through the whole device layer with high field intensity and is reflected back from the buried oxide interfaces. The multiple reflections in the cavities leads to enhanced interaction of incident light with the scattering nanostructure and, thus, to increased coupling. In addition to the broadband enhancement, the fine-structure of the spectra in Figs. 2a-d can be attributed to the interaction of the plasmonic nanostructures with the substrate. To demonstrate this, Fig. 2f depicts the responsivity data (for devices with and without nanodots) from which the absorption enhancement is calculated for Fig. 2d. It can be seen that the spectrum for the device without nanodots is very similar to the simulated spectra shown in Fig. 2e, while the curve with nanodots show – in addition to the broadband enhancement – some fine-structure and deviation of the symmetry of the peaks. In the theoretical curves the fine-structure is evident as strong peaks that may be attributed to the waves coupled to the SOI waveguide modes and to the modal cutoff conditions of the waveguide [17]. Near the cutoff the waveguide and plasmonic modes have the biggest overlap and, thus, the strongest coupling between the resonances. Therefore peak positions depend strongly on the thickness of the SOI layers but are also influenced by the parameters of the plasmonic nanostructures. To further illustrate the influence of the different nanodot arrays, Fig. 3 depicts the calculated reflectance spectra of the 2200 nm SOI substrate with the three nanostructures

of Fig. 2. The same SOI substrate without nanodots is shown as a reference. In Fig 3c the influence of an 80 nm thick silicon nitride (Si_3N_4) anti-reflection coating is also displayed for comparison. It can be seen that all the three nanostructures generate a broadband – but somewhat different – decrease in the reflectance spectra as compared with the substrate without the dots. In addition, sharp dips are observed in the reflectance spectra corresponding to the sharp peaks in the theoretical absorption enhancement spectra of Figs. 2a, 2b and 2d. When the incoming radiation is favourably scattered by the plasmonic nanoparticles towards the substrate, the reflectance is reduced. When scattered to the propagation angles exceeding that of the total internal reflection, light may remain trapped in the SOI device layer and couple to the waveguide modes, which significantly increases the effective path of light in the absorbing Si layer and, thus, the probability for absorption. This is illustrated in Fig. 4 where the absorption profile, computed for the spectral peak at 996 nm of Fig. 2a, implies that the light propagates in the in-plane (x) direction and is, thus, coupled to a waveguide mode. The correspondence of the spectral peak wavelength with the propagating wavelength indicates that the scattered light is efficiently coupled with the guided mode, resulting in enhanced optical paths lengths in Si and, thus, in the absorption enhancement. The enhanced standing wave pattern visible in Fig. 4 shows the high absorption (high field) regions (anti-nodes) in the Si waveguide.

The spectral absorption enhancement profiles, shown in Figs. 2a-d, are, thus, a combined effect of the favourable scattering of light by the plasmonic nanoparticle arrays into the SOI device layer, coupling to the waveguide modes interacting with the plasmonic array and of the interference phenomena in the Farby-Pérot cavities of the SOI multilayer structure. It should be noted that even though the simulated absorption enhancement may remain slightly below one for the wavelengths at the minima of the Fabry-Pérot oscillations (corresponding to the destructive Fabry-Perot interferences) the plasmonic enhancement is able to keep the total integrated plasmonic contribution clearly beneficial for the range of wavelengths studied (note the logarithmic scale in Figs. 2a-d).

To further study the absorption enhancements in SOI structures, a photovoltaic device was prepared on a SOI wafer with h_{SOI} = 300 nm and h_{BOX} = 3000 nm. In Fig. 5 the experimental and simulated absorption enhancements are shown for Ag nanodots with d = 200 nm arranged in a square matrix with p = 470 nm on a 30 nm top oxide layer. Again, variations from the nominal thickness of the device layer are observed: A good match between the peak positions of the experimental and simulated results can be obtained when h_{SOI} in the simulation is set to 280 nm (Fig. 5a), while for the nominal thickness of h_{SOI} = 300 nm significant shifts in the peak positions are observed (Fig. 5b). Fig. 5c shows the influence of the thickness variations on the spectral peak positions of the fraction of light absorbed in the simulated SOI device layers with h_{SOI} = 280 and 300 nm without the Ag nanostructures on top. The maximum absorption enhancement of the simulated structures on the semi-infinite substrates remains slightly below 1.5 in Fig. 5, while the value for the SOI structure is as high as 75 and the maximum for the experimental photocurrent enhancement is about 20.

It should be noted that the above reported plasmon-induced enhancements in SOI structures are also significantly higher than those reported for the thin-film solar cells of amorphous Si with a metal back contact reflector [9]. This can be understood by the fact that light absorption in crystalline Si is considerably weaker than that in amorphous Si and, thus, a significant amount of energy is able to pass the SOI device layer to the interface of buried oxide where the waves are reflected back resulting to the Fabry-Pérot interference and intensive field oscillations, in addition to coupling to the waveguide, while even in fairly thin amorphous Si films only weak Fabry-Pérot resonances can be seen only at very long wavelengths.

Conclusions

We have shown both theoretically and experimentally that plasmonic nanostructures based on periodic Ag nanoparticle arrays can generate a remarkable absorption enhancement in SOI substrates compared to that in semi-infinite or thick substrates. According to the theoretical calculations, absorption enhancements at long wavelengths - close to the Si band gap where the light absorption in Si is low - can be as high as 80, while the maximal experimental photocurrent enhancements were demonstrated to reach the values of about 12 and 20 for the non-optimised photoconductive and photovoltaic SOI test structures in which high losses in the carrier collection efficiencies are expected. The spectral features of the absorption enhancements observed both experimentally and theoretically were attributed to several different interacting resonant phenomena: the favourable scattering of the normally incident light by the periodic plasmonic nanoparticle arrays into the SOI device layer, coupling to the waveguide modes interacting with the plasmonic array and the interference phenomena in the Farby-Pérot multilayer cavities.

Acknowledgements

The authors wish to thank O. Hahtela and J. Leppäniemi for their help in sample preparation and A. Akujärvi for his guidance in running the monochromator. The Academy of Finland and VTT Technical Research Centre of Finland are gratefully acknowledged for funding.

References

1. Stuart HR, Hall DG (1998) Island size effects in nanoparticle-enhanced photodetectors. Appl Phys Lett 7:3815-3817

2. Sopori B (2003) Thin-film Silicon Solar Cells. In: Luque A, Hegedus S (eds) Handbook of Photovoltaic Science and Engineering, 2nd edn. John Wiley & Sons, ISBN: 0-471-49196-9, pp 307-357

3. Green MA (2004) Recent developments in photovoltaics. Sol. Energy, 2004, 76, 3-8
4. Yablonovitch E, Cody GD (1982) Intensity enhancement in textured optical sheets for solar cells. IEEE Trans Electron Devices ED-29:300-305
5. Campbell P, Green MA (2001) High performance light trapping textures for monocrystalline silicon solar cells. Sol Energy Mater Sol Cells 65:369-375
6. Atwater HA, Polman A (2010) Plasmonics for improved photovoltaic devices. Nat Mat 9:205–213
7. Schaadt DM, Feng B, Yu ET (2005) Enhanced semiconductor optical absorption via surface plasmon excitation in metal nanoparticles. Appl Phys Lett 86:063106
8. Beck FJ, Polman A, Catchpole KR (2009) Tunable light trapping for solar cells using localized surface plasmons. J Appl Phys 105:114310
9. Akimov YA, Koh WS (2011) Design of plasmonic nanoparticles for efficient subwavelength light trapping in thin-film solar cells. Plasmonics 6:155-161
10. Spinelli P, Ferry VE, van de Groep J, van Lare M, Verschuuren MA, Schropp REI, Atwater HA, Polman A (2012) Plasmonic light trapping in thin-film Si solar cells. J Opt 14:024002
11. Enderlein J, Ruckstuhl T, Seeger S (1999) Highly efficient optical detection of surface-generated fluorescence. Appl Optics 38:724-732
12. Välimäki H, Tappura K (2009) A novel platform for highly surface-sensitive fluorescent measurements applying simultaneous total internal reflection excitation and super critical angle detection. Chem Phys Lett 473:358-362
13. Stuart HR, Hall DG (1996) Absorption enhancement in silicon-on-insulator waveguides using metal island films. Appl Phys Lett 69:2327-2329
14. Stuart HR, Hall DG (1998) Enhanced dipole-dipole interaction between elementary radiators near a surface. Phys Rev Lett 80: 5663-5666
15. Earl SK, Gómez DE, James TD, Davis TJ, Roberts A (2015) Material effects on V-nanoantenna performance. Nanoscale 7:4179-4186
16. Mokkapati S, Beck FJ, Polman A, Catchpole KR (2009) Designing periodic arrays of metal nanoparticles for light-trapping applications in solar cells. Appl Phys Lett. 95:053115.
17. Soller BJ, Hall DG (2001) Energy transfer at optical frequencies to silicon based waveguiding structures. J Opt Soc Am A 18:2577-2584
18. Pillai S, Catchpole KR, Trupke T, Green MS (2007) Surface plasmon enhanced silicon solar cells. J Appl Phys 10: 093105.
19. Ono A, Enomoto Y, Matsumura Y, Satoh H, Inokawa H (2014) Broadband absorption enhancement of thin SOI photodiode with high-density gold nanoparticles. Opt Mater Express 4:725-732
20. Ferry VE, Sweatlock LA, Pacifici D, Atwater HA (2008) Plasmonic nanostructure design for efficient light coupling into solar cells. Nano Lett 8:4391-4397
21. www.comsol.com.
22. Palik ED, Handbook of Optical Constants of Solids, Vol. I. Academic Press, Orlando,1985.

23. http://www.sspectra.com/sopra.html
24. Johnson PB, Christy RW (1972) Optical constants of noble metals. Phys Rev B 6:4370-4379
25. Green MA (2008) Self-consistent optical parameters of intrinsic silicon at 300 K including temperature coefficients. Sol Energy Mater Sol Cells 92:1305-1310
26. Burkhard GF, Hoke ET, McGehee MD (2010) Accounting for interference, scattering, and electrode absorption to make accurate internal quantum efficiency measurements in organic and other thin solar cells. Adv Mater 22:3293-3297
27. Card H (1976) Aluminum-silicon Schottky barriers and ohmic contacts in integrated circuits. IEEE Trans Electron Devices ED-23:538-544
28. Elhadidy H, Sikula J, Franc J (2011) Symmetrical current–voltage characteristic of a metal–semiconductor–metal structure of Schottky contacts and parameter retrieval of a CdTe structure. J Semicond Sci Technol 27:015006.
29. Lim SH, Mar W, Matheu P, Derkacs D, Yu ET (2007) Photocurrent spectroscopy of optical absorption enhancement in silicon photodiodes via scattering from surface plasmon polaritons in gold nanoparticles J Appl Phys 101:104309

Figures

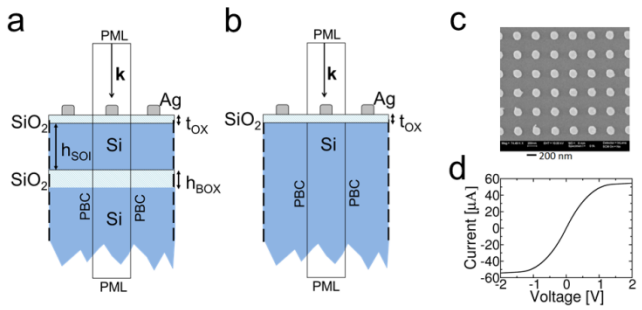

Fig. 1 Cross sectional schematic views of the simulated 3D systems with Ag nanoparticles on (a) a SOI and (b) semi-infinite crystalline Si substrate with a thin top SiO_2 layer. t_{OX} is the thickness of the top oxide, h_{SOI} that of the SOI device layer and h_{BOX} is the thickness of the buried oxide. The wave vector, **k**, indicating the direction of the incident plane wave is shown inside a rectangular box representing the boarders of the simulation box, on the vertical sides of which the periodic boundary conditions (PBC) are applied. The handle wafer below the buried oxide is assumed semi-infinite or thick enough to absorb all the power that may enter in it. (c) A scanning electron microscope image of a nanodot array with d = 180 nm and p = 420 nm. (d) A typical IV curve of the photoconductive samples (the linear low bias region is applied for the photoconductive measurements)

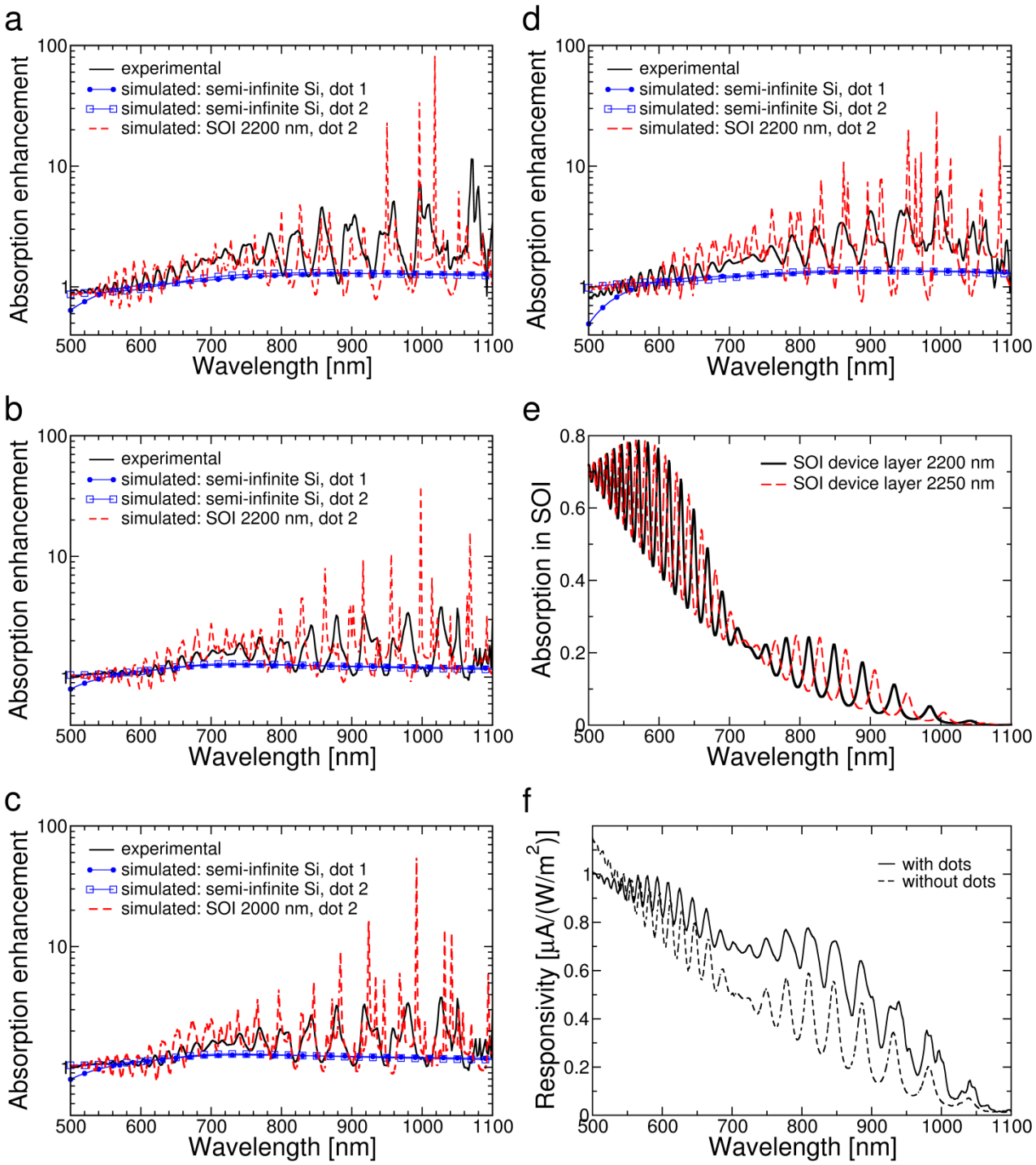

Fig. 2 (a-d) Plasmon-induced absorption (simulation) and photocurrent (experimental) enhancement in a semi-infinite substrate and in the SOI device layer of a structure where the nominal thicknesses of the experimental samples are: t_{OX} = 50 nm, h_{SOI} = 2200 nm, h_{BOX} = 500 nm. For the Ag nanodots d = 150 nm in (a-c) and 180 nm in (d) and p = 350 nm in (a), 450 nm in (b-c) and 420 nm in (d). In the simulations h_{SOI} is 2200 nm in (a-b) and (d) and 2000 nm in (c). Dot 1 corresponds to sharp cylindrical Ag nanodots and dot 2 to that with a rounded top. (e) The simulated fraction of the incident power absorbed in the SOI device layers of h_{SOI} = 2200 nm (black) and h_{SOI} = 2250 nm (red) without nanodots. (f) The measured responsivities of the samples with nanodots (d = 180 nm, p = 420 nm) and without nanodots

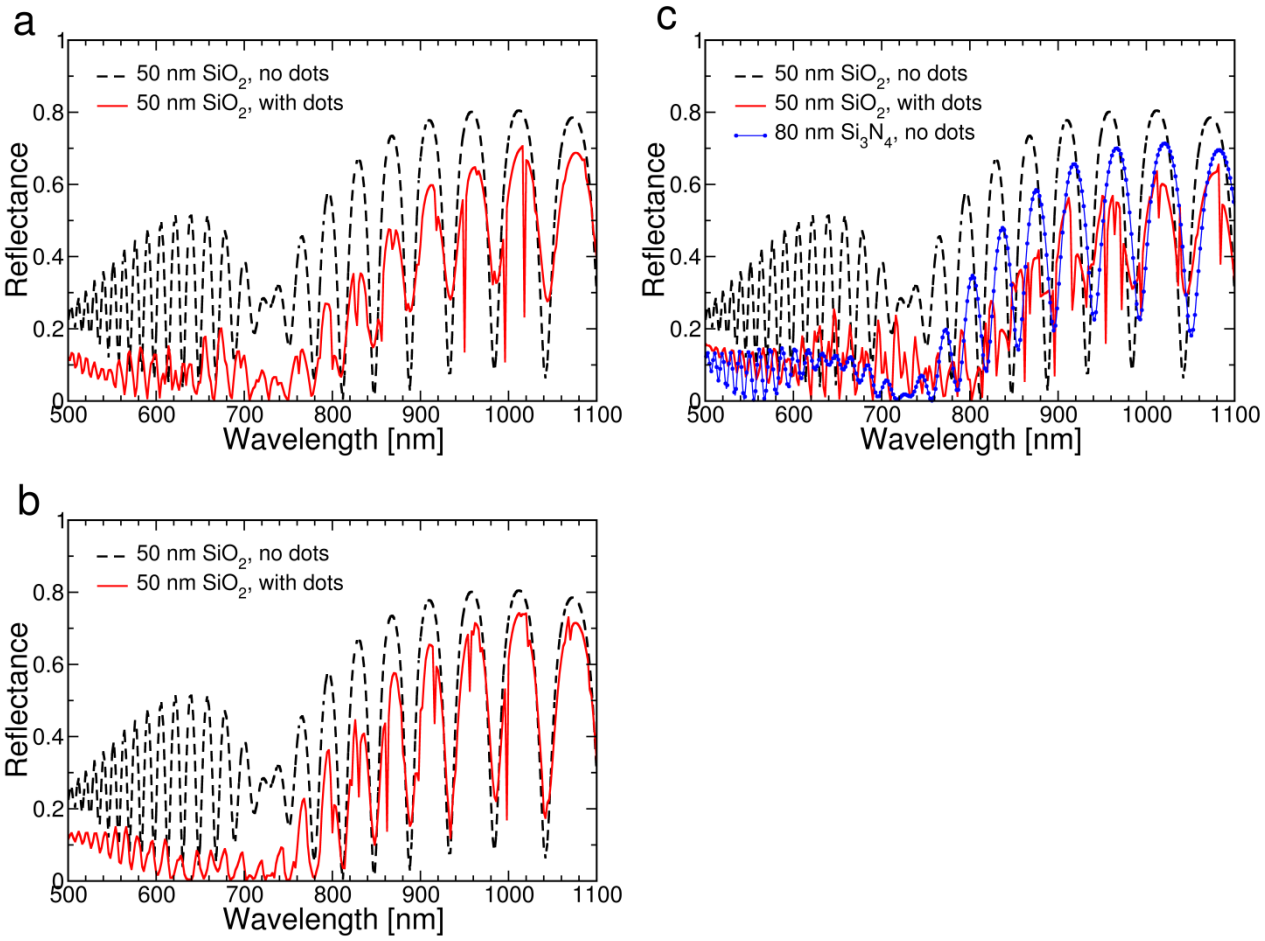

Fig. 3 Calculated reflectance spectra of the 2200 nm SOI substrate (t_{OX} = 50 nm, h_{SOI} = 2200 nm, h_{BOX} = 500 nm) with the three nanostructures of Fig. 2 (solid red lines). The same SOI substrate without nanodots is shown as a reference (dashed line). (a) d = 150 nm, p = 350 nm, (b) d = 150 nm, p = 450 nm, (c) d = 180 nm, p = 420 nm. The influence of an 80 nm thick Si_3N_4 anti-reflection coating replacing the SiO_2 spacer layer is also shown in (c)

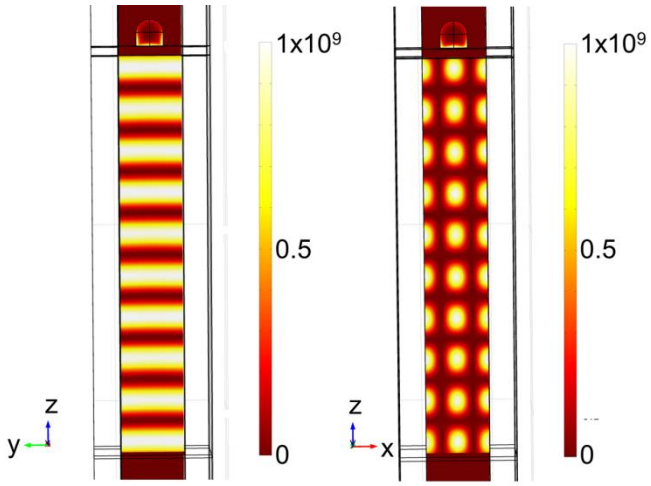

Fig. 4 Coupling (a normally incident *y*-polarized plane wave) to a waveguide mode with an enhanced standing wave in the SOI layer: Two orthogonal cross sectional views of the total power dissipation (i.e. absorption, in W/m^3) at the wavelength of 996 nm for the same simulated SOI structure for which the absorption enhancements are shown in Fig. 2a. The 2 nm Cr adhesion layer under the Ag nanodot generates significant – although not fatal – absorption losses. The maximum value of the colour scales is set to 1×10^9 W/m^3 for visual clarity

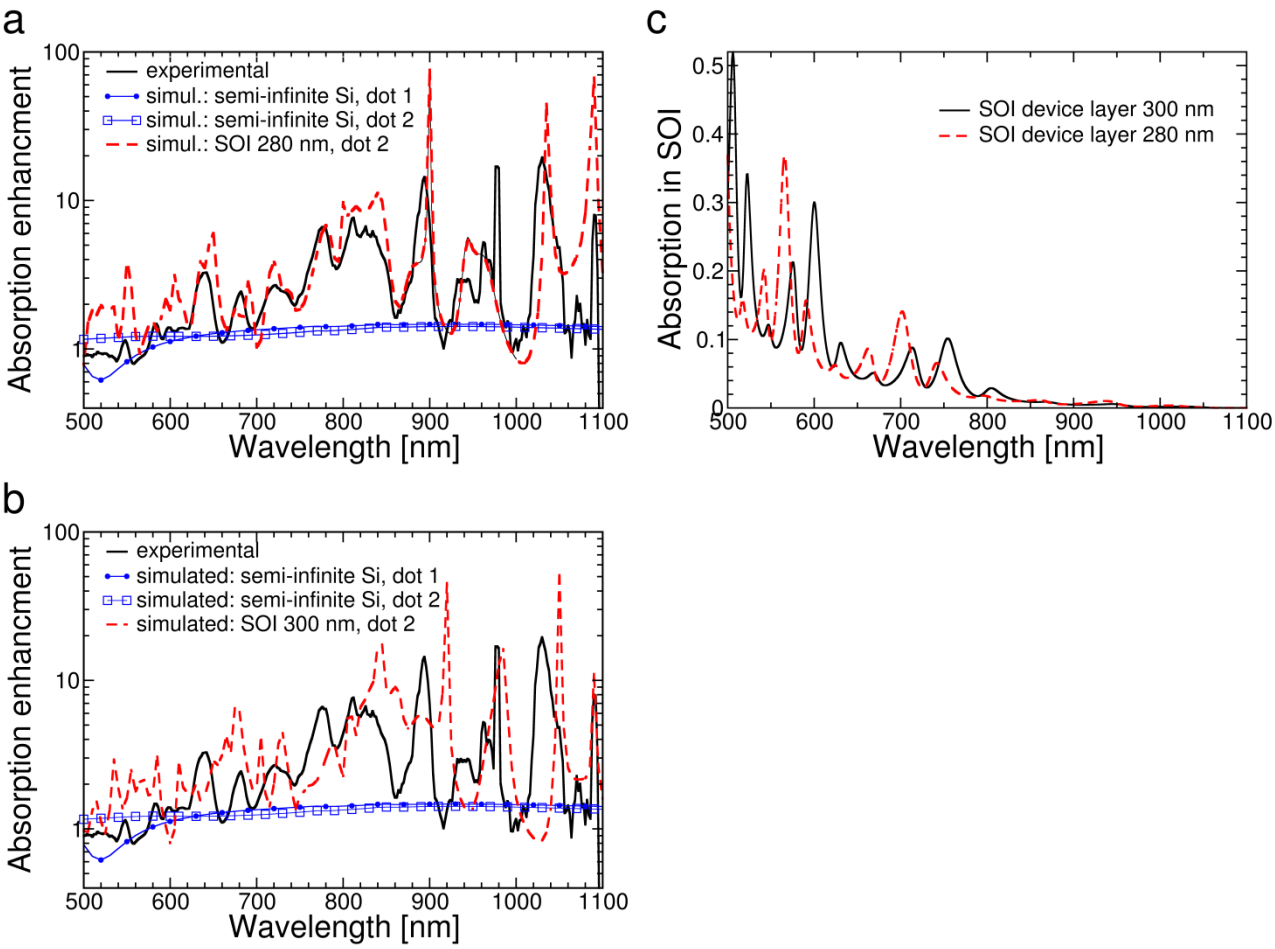

Fig. 5 (a)-(b) Plasmon-induced absorption (simulation) and photocurrent (experimental) enhancements in a semi-infinite substrate and in the SOI device layer of a structure where the nominal thicknesses are: t_{OX} = 30 nm, h_{SOI} = 300 nm, h_{BOX} = 3000 nm. The Ag nanodots (d = 200 nm) form a square matrix with p = 470 nm. In the simulations h_{SOI} = 280 nm in (a) and 300 nm in (b). Dot 1 corresponds to sharp cylindrical Ag nanodots and dot 2 to that with a rounded top. (c) The simulated fraction of the incident power absorbed in the SOI device layers of h_{SOI} = 300 nm (black) and h_{SOI} = 280 nm (red) without nanodots